JACS
JOURNAL OF THE AMERICAN CHEMICAL SOCIETY
pubs.acs.org/JACS
Article

Structural Transformation in a Sulfurized Polymer Cathode to Enable Long-Life Rechargeable Lithium−Sulfur Batteries

Shen Wang,[⊥] Bingyu Lu,[⊥] Diyi Cheng, Zhaohui Wu, Shijie Feng, Minghao Zhang, Weikang Li, Qiushi Miao, Maansi Patel, Jiaqi Feng, Emma Hopkins, Jianbin Zhou, Saurabh Parab, Bhargav Bhamwala, Boryann Liaw, Ying Shirley Meng,* and Ping Liu*

Cite This: https://doi.org/10.1021/jacs.3c00628
Read Online
ACCESS | Metrics & More | Article Recommendations | Supporting Information

ABSTRACT: Sulfurized polyacrylonitrile (SPAN) represents a class of sulfur-bonded polymers, which have shown thousands of stable cycles as a cathode in lithium−sulfur batteries. However, the exact molecular structure and its electrochemical reaction mechanism remain unclear. Most significantly, SPAN shows an over 25% 1st cycle irreversible capacity loss before exhibiting perfect reversibility for subsequent cycles. Here, with a SPAN thin-film platform and an array of analytical tools, we show that the SPAN capacity loss is associated with intramolecular dehydrogenation along with the loss of sulfur. This results in an increase in the aromaticity of the structure, which is corroborated by a >100× increase in electronic conductivity. We also discovered that the conductive carbon additive in the cathode is instrumental in driving the reaction to completion. Based on the proposed mechanism, we have developed a synthesis procedure to eliminate more than 50% of the irreversible capacity loss. Our insights into the reaction mechanism provide a blueprint for the design of high-performance sulfurized polymer cathode materials.

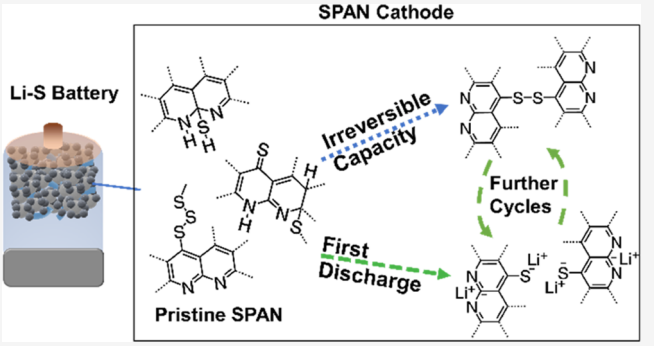

1. INTRODUCTION

Lithium−sulfur (Li−S) batteries are being extensively studied as they are promising for a wide range of applications from powering portable electronic devices to electric vehicles.[1−4] The low cost and abundance of sulfur, along with its high theoretical capacity, make it a compelling alternative to conventional metal oxides. However, challenges for sulfur cathodes are well documented: sulfur has exceptionally low conductivity ($\sim 10^{-24}$ S cm^{-1})[3] and the formation of soluble polysulfide intermediates (Li_2S_x) during discharge results in capacity loss ("shuttle effect") as well as poor Coulombic efficiency.[4] The involvement of electrolytes in the cathode reaction also makes the electrochemical performance sensitive to the electrolyte amount.[5]

To improve the conductivity and minimize the "shuttle effect" in Li−S batteries, sulfurized polymers have been investigated, where sulfur is covalently bonded to polymer backbones.[6−10] Sulfurized polyacrylonitrile (SPAN) is the best-known example, which is synthesized by heating elemental sulfur and polyacrylonitrile (PAN) in an inert gas condition.[11,12] Recently, with a highly concentrated salt/ether electrolyte diluted in a fluorinated ether, SPAN has been shown to be stable for over 1200 cycles.[13] Moreover, its capacity is further enhanced by approaches such as doping, precursor modification, or with a sealed reaction container.[14−17] Finally, SPAN has also shown promise as a cathode in solid-state batteries.[18]

Although SPAN was discovered as a battery cathode in 2002, its structure and charge storage mechanism are not clearly depicted in previous literature. SPAN was initially postulated as a mixture of fused pyridine ring polymers with physically adsorbed elemental sulfur,[11,19] a model that is still beheld today.[15,20,21] Soon after, covalent C−S bonds were observed, suggesting that SPAN is a sulfur-bonded polymer.[22] Over the years, more functional groups have been identified, including bridging sulfur chain ($-S_x-$, $x < 4$), thioketone (C=S), and N−H along with short-chain sulfur species S_2 and S_3 bonded to a fused pyridine polymer backbone,[12,23] which prevents the formation of longer chain polysulfides responsible for the shuttle effect during cycling. Recent studies have proposed the existence of N−S bonds (1′-pyridine sites), while some sulfur atoms are bonded at the 2′-pyridine sites.[24−26]

Received: January 17, 2023

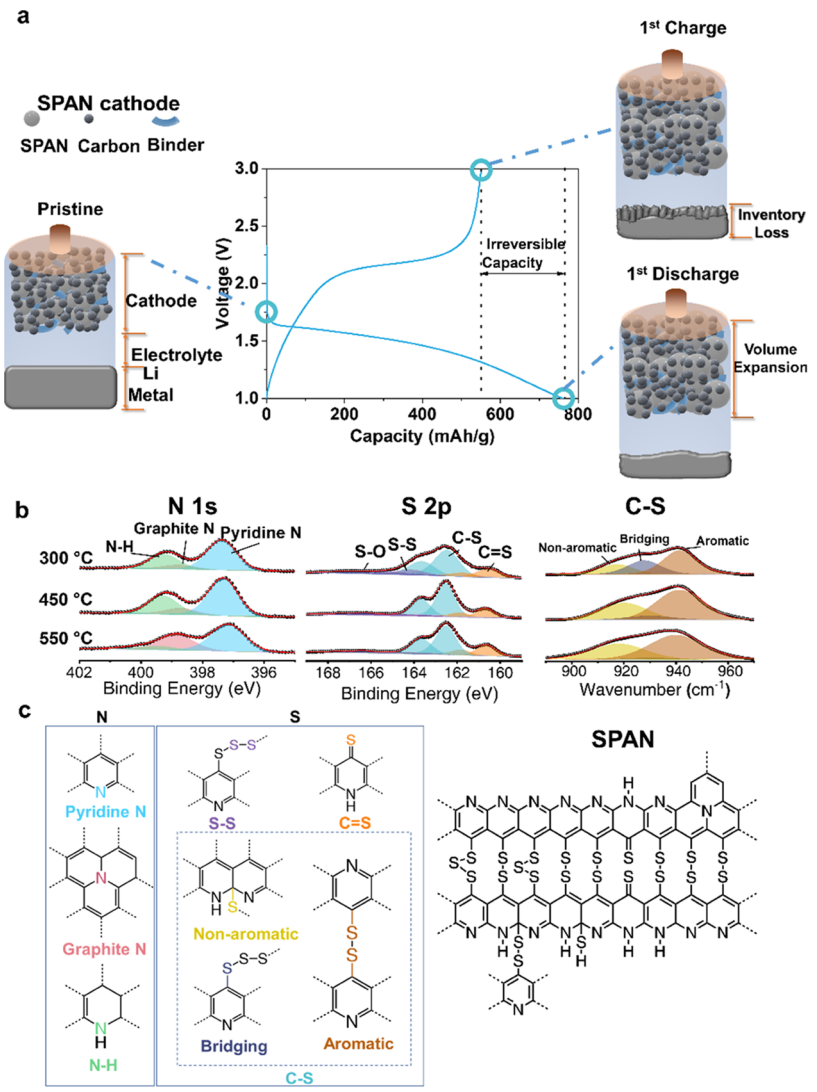

Figure 1. Irreversible capacity loss and structure of SPAN. (a) Schematic of SPAN's irreversible capacity loss in the battery; (b) high-resolution X-ray photoelectron spectroscopy (XPS) N 1s, S 2p, and deconvoluted C−S FTIR for SPAN synthesized from 300 to 550 °C; and (c) summary of components and the proposed structure of SPAN.

Researchers have also explored the reversible operating mechanism of SPAN. A 2018 study proposed that a SPAN structure consists of a fused pyridine ring backbone cross-linked by S−S.[27] During discharge, the polymer backbone with its covalently bonded sulfur has two lithium host sites per unit (C_3NS): one is associated with the fused pyridine ring's N−C═N, and the other is associated with S, which is cleaved from the "S−S" in the pyridine−S−S−pyridine (C−S−S−C) structure.

Despite the significant progress in understanding the SPAN structure and charge storage mechanism, its irreversibility during the 1st cycle remains unresolved: persistently an over 25% irreversible capacity loss and lower discharge potentials than in subsequent cycles.[12] After the 1st cycle, SPAN exhibits exceptional stability in cycling. As shown in Figure 1a, excess Li in the anode is required to compensate for the loss during the 1st cycle, which undermines the cell energy density. Moreover, the 1st cycle irreversibility also creates over 20% volume expansion,[28] which may lead to electrode cracking and delamination. Understanding the nature of the chemical and structural transformation during the 1st cycle is crucial for SPAN's application in batteries, which can provide structural design guidelines for polymer cathode materials in general. In a previous study, the formation of Li−C−N−Li[29,30] or Li−C−C−Li[30] after the 1st discharge has been proposed to account for the irreversible capacity. These species are suggested to enhance the conductivity of the polymer in the following cycles.

In this work, we characterize each functional group's role in the SPAN reaction during the 1st cycle based on a reconstructed SPAN structure. A SPAN thin film is fabricated to remove the interference from the conductive carbon and binder during characterization. This enables the study of the interfacial compositions, direct measurement of electronic conductivity, and the detection of intermediates during the cycling process. The results suggest that the cause for the 1st cycle irreversible capacity loss is the increase in aromaticity of the SPAN polymer backbone through the transformation of the nonaromatic functional groups into conjugated conductive pathways. Meanwhile, the conductive carbon in typical composite electrodes plays a facilitating role in transforming the reaction intermediates into the conjugated path during the

https://doi.org/10.1021/jacs.3c00628
J. Am. Chem. Soc. XXXX, XXX, XXX−XXX

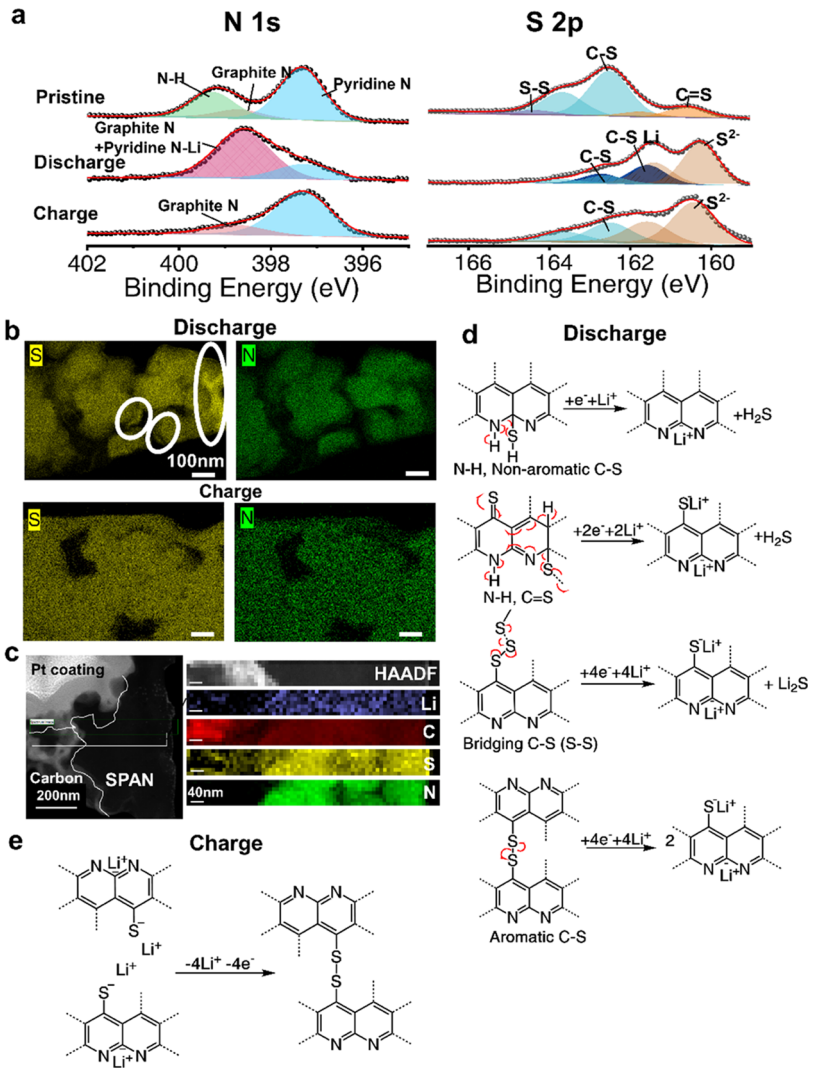

Figure 2. Roles of SPAN functional groups during the 1st cycle. (a) N 1s and S 2p XPS spectra of the SPAN cathode before and after the 1st cycle; (b) STEM−EDX mapping (sulfur and nitrogen) of the SPAN cathode after the 1st cycle in the cell; and (c) STEM−electron energy loss spectroscopy (EELS) of the SPAN cathode after the 1st discharge in the cell; and the proposed working mechanism of each nitrogen and sulfur component in SPAN in the 1st: (d) discharge and (e) charge.

1st cycle. The working mechanism for the 1st and subsequent cycles motivated us to develop a post-thermal treatment to reduce the nonaromatic component in SPAN. As a result, the 1st cycle irreversible capacity loss is reduced by more than 50%. With these understandings of the SPAN reaction mechanism, the future direction of the SPAN cathode development is discussed and a blueprint for the development of highly reversible sulfur-containing polymers for batteries is proposed.

2. RESULTS AND DISCUSSION

2.1. Structure of SPAN. First, we construct a structural model for the SPAN synthesized in this work. Three SPAN samples were synthesized at 300, 450, and 550 °C, respectively. Analysis of the ratio of the functional groups as a function of temperature helped to elucidate the structural model. The elements (C, N, and S) in SPAN are uniformly distributed, as shown by scanning transmission electron microscopy−energy-dispersive X-ray spectroscopy (STEM−EDX) images (Figure S1). The elemental analysis results are listed in Table S1.

In the SPAN N 1s XPS spectra (Figure 1b), three peaks at 397.2, 398.7, and 399.5 eV are assigned to pyridine-*N*, graphite-*N*, and N−H, respectively (Figure 1c). In the S 2p XPS spectra (Figure 1b), the peaks at 160.5, 162.5, and 164.2 eV are assigned to C═S, C−S, and bridging S−S, respectively (Figure 1c). As temperature increases, the bridging S−S diminishes with higher synthesis temperature. A more detailed analysis concerning peak assignments is explained in the Supporting Information, "SPAN Structure Reconstruction" section.

To further study the nature of the C−S bonds, the C−S peak in Fourier-transform infrared spectra (FTIR) is deconvoluted in Figure 1b. Three Gaussian peaks are identified, which represent the aromatic C−S (940 cm^{-1}), nonaromatic C−S (918 cm^{-1}), and C−S bonded with bridging sulfur (C−S_x, 928 cm^{-1}) (Figure 1c). Based on these results, we propose the functional groups and the SPAN structure, as shown in Figure 1c. In general, this structure is close to the SPAN model proposed by Buchmeiser et al.,[23] but contains the nonaromatic C−S[25] and graphite-*N*.

https://doi.org/10.1021/jacs.3c00628
J. Am. Chem. Soc. XXXX, XXX, XXX−XXX

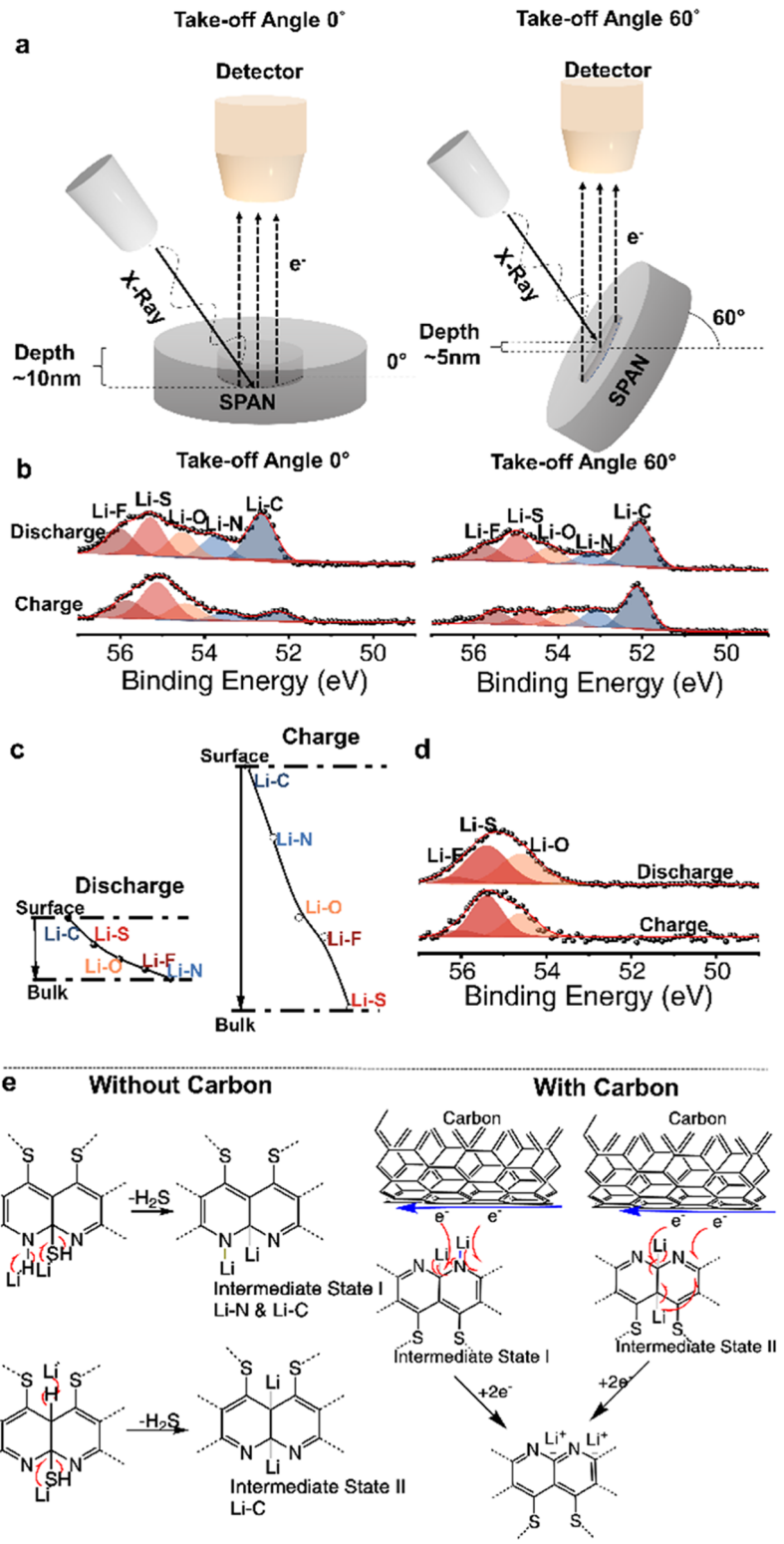

Figure 3. Intermediates of the SPAN lithiation reaction. (a) Schematic of the angle-resolved XPS (AR-XPS) for testing the thin-film SPAN cathode; (b) AR-XPS Li 1s for the thin-film SPAN cathode (without carbon) before and after the 1st discharge and charge; (c) relative depth profiling of the SPAN cathode electrolyte interphase (CEI) after the 1st discharge and charge; (d) XPS Li 1s for the SPAN cathode (SPAN (80%)/CMC (10%)/carbon black (10%)) before and after the 1st discharge and charge in a cell; and (e) proposed reaction mechanism for the SPAN without/with carbon during the discharge.

2.2. Roles of Functional Groups in SPAN during the 1st Cycle. We then examine the roles of functional groups during the 1st cycle of the SPAN synthesized at 450 °C, which has shown the best electrochemical performance (Figure S4). In Figure 2a, the disappearance of the XPS N 1s peak indicates that the N−H group is irreversibly converted to other functional groups during the 1st discharge. The pyridine-*N* undergoes reversible changes, with its intensity decreasing

https://doi.org/10.1021/jacs.3c00628
J. Am. Chem. Soc. XXXX, XXX, XXX−XXX

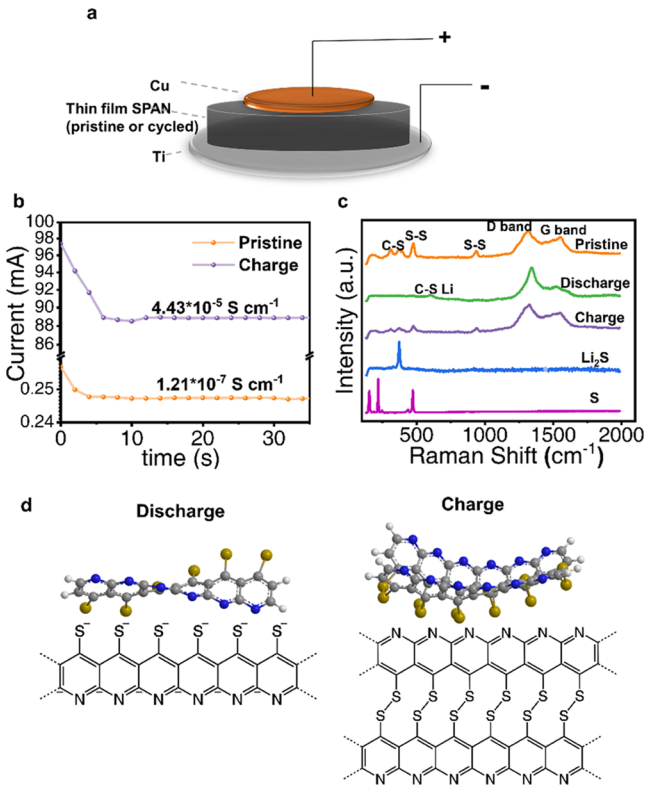

Figure 4. SPAN structure after the 1st cycle. (a) Schematic and (b) results of the electrical conductivity test for the SPAN thin film before and after the 1st cycle; (c) Raman spectra of the pristine SPAN cathode after the 1st discharge and after the 1st charge; and (d) proposed structure for the main discharge/charge products for SPAN.

upon discharge and recovering upon charge. This phenomenon is reasonable since the fused pyridine N−C═N site can host lithium, which causes the peak to shift to a higher binding energy region, close to where the graphite-*N* peak is.[27] There is no obvious position change for the graphite-*N* peak itself, indicating that the graphite-*N* is intact during cycling.

Figure 2a also shows the evolution of the S 2p spectra: the long chain S−S (164.2 eV) is irreversibly lost during the 1st discharge. Previous studies introduced well-dispersed long-chain sulfur in SPAN by a physical adsorption method. This long-chain sulfur can convert to Li_2S after discharge and contributes to an enhanced reversible capacity.[15] However, results in Figure 2a indicate that Li_2S generated by long-chain sulfur does not appear to be reversible since the 164.2 eV peak did not recover after charge. C═S (160.5 eV) is also irreversibly lost, consistent with our previous report.[16] A new peak at 160.2 eV emerges, which is attributed to the S^{2-} species. These species have a similar peak position to C═S.[25] On the other hand, the C−S peak at 162.5 eV decreases during the 1st discharge, while a new peak at 161.6 eV emerges. During charge, this 161.6 eV peak disappears, while the peak at 162.5 eV amplifies. The partially reversible change between these two peaks indicates a redox process between C−S−S−C and C−S^- Li^+. However, we note that this C−S−S−C redox process is not completely reversible as the area of the 162.5 eV peak does not fully recover. Meanwhile, XPS survey spectra in Figure S5 indicate that the S/N ratio changes from 1.09 (pristine) to 1.38 (discharged) and further to 0.90 (charged). The change in the S/N ratio indicates that sulfur accumulates on the cathode/electrolyte interface during the 1st discharge, leading to permanent sulfur loss after the charge. Similar phenomena have been observed in the STEM−EDX (Figure 2b), which indicates sulfur accumulation at the interface after the 1st discharge, but sulfur distribution is uniform after its 1st charge. More STEM−EDX images are provided in Figure S6.

To further understand the origin of the interfacial accumulation of sulfur after discharge, we conducted chemical lithiation of SPAN to simulate the discharge product.[31] The analysis of the evolved gas confirmed H_2S formation by gas chromatography−mass spectrometry (GC−MS) (Figure S7). This indicates that a portion of sulfur is irreversibly lost during the first discharge. Further, lithiated SPAN acts as a Lewis base to absorb the generated H_2S at the surface. Upon charge, the Lewis basicity of SPAN is expected to decrease when H_2S is released. The formation and migration of H_2S are further corroborated by the STEM−electron energy loss spectroscopy (STEM−EELS) images (Figure 2c). After the 1st discharge, most of the sulfur in SPAN remains in the solid matrix, while some sulfur is found to have diffused into the conductive carbon additive. Moreover, sulfur distribution in the conductive carbon does not correlate with that of lithium, indicating that it is not Li_2S. This observation is consistent with the presence of H_2S. The residual hydrogen (Table S1) in SPAN is likely the hydrogen source for the H_2S formation.

Although the irreversible formation and loss of H_2S have been observed upon lithiation, the chemical identity of the sulfur source in SPAN is still unidentified. Since the dominant S components in SPAN are C−S (Figures 1b and S2a) and the aromatic C−S is reversible, it is highly likely that the formation of H_2S is from the nonaromatic C−S species. This explains why some of the C−S is permanently lost upon charge, as evidenced by XPS (S 2p in Figure 2a). In contrast to the complex behavior of S, no nitrogen segregation is observed in STEM−EDX results despite the disappearance of N−H after the 1st discharge. This indicates that all of the nitrogen in the SPAN reacted without dissociation.

Based on these analyses, the following mechanism for the SPAN 1st discharge is proposed (Figure 2d). The N−H group is converted into aromatic pyridine-*N* via deprotonation; the formation of H_2S is due to the loss of nonaromatic C−S; the C═S is converted into aromatic C−S, and the long S−S chain is cleaved. As far as the C−S on an aromatic structure, the cross-linked S−S bond is cleaved and lithiated. The formation of H_2S is responsible for the irreversible capacity loss. Li_2S, on the other hand, may still participate in subsequent cycling. During charge (Figure 2e), the fused pyridine backbone can re-cross-link through the formation of C−S−S−C.

2.3. Role of Conductive Carbon in a SPAN Cathode.

To gain additional insights into the charge storage mechanism, we developed a thin-film SPAN electrode that is free of conductive carbon. More information regarding its synthesis and characterizations are in the Supporting Information, "Thin Film SPAN Synthesis and Characterization" section. As shown in Figure 3a, the use of a thin film enables the application of angle-resolved XPS (AR-XPS) to probe the compositional depth profile of the electrode after the 1st cycle: at 0° take-off angle, the estimated maximum probing depth is 10 nm, and at 60° take-off angle, the probing depth is 5 nm.[32] Unlike the XPS plasma depth-profiling method, AR-XPS is nondestructive, which minimizes the etch-induced artifacts.

The Li 1s AR-XPS spectra are displayed in Figure 3b. In addition to the common CEI components such as Li−O, Li−S, and Li−F, two extra peaks are observed at binding energies

https://doi.org/10.1021/jacs.3c00628
J. Am. Chem. Soc. XXXX, XXX, XXX−XXX

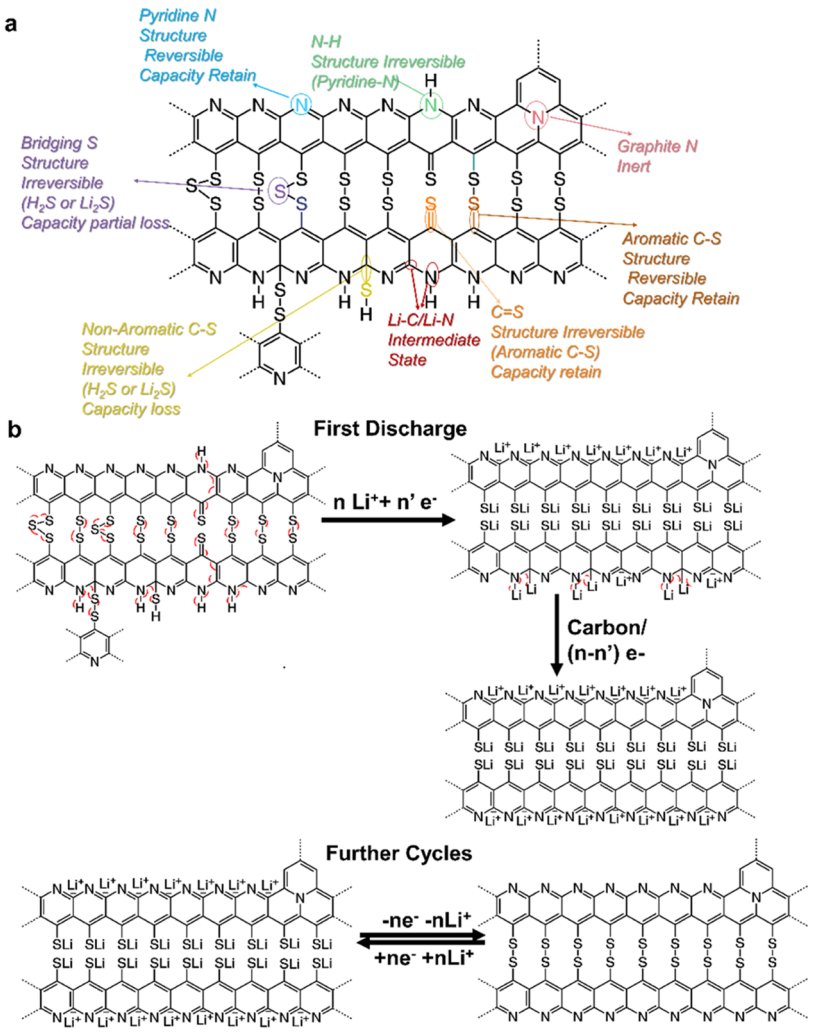

Figure 5. Working mechanism for SPAN in a battery. (a) Summary of the role of functional groups in SPAN and (b) proposed SPAN working mechanism.

lower than 54 eV, the value for the Li metal. A possible explanation for this surprising observation is the formation of covalent Li−N and Li−C bonds, which had been proposed previously.[29,30] The lower electronic negativity for C (compared to N) makes it reasonable to assign the peak at 52.2 eV to Li−C and the peak at 53.2 eV to Li−N. The relative depth of Li components is estimated by comparing the value $\mathrm{Ln}(I_{60^\circ}/I_{0^\circ})$ for each peak in the AR-XPS. I_{degree} is the peak intensity of the components at a certain angle.[32] A relative depth plot is shown in Figure 3c. Compared to the discharge results where N−Li and C−Li are more uniformly distributed with other lithium components, after charge, the N−Li and C−Li components are preferentially accumulated on the SPAN surface. On the other hand, in Figure 3d, these two N−Li and C−Li components have not been observed when the conductive carbon is added to the SPAN electrode. Therefore, the surface accumulation of the N−Li and C−Li bonds in thin-film SPAN might be due to the low surface electronic conductivity. When conductive carbon is added, there are sufficient electrons to react with the N−Li and C−Li to complete the SPAN lithiation reaction. Thus, the N−Li and C−Li components only exist as intermediates in thin-film SPANs but not in the presence of conductive carbon. While Li−C−N−Li[29,30] and Li−C−C−Li[30] species were suggested to permanently remain in the SPAN structure after the 1st discharge, our observations suggest that these components are intermediates. A N−Li intermediate species, with a peak at 398.2 eV (Figure S9a), is also observed in the AR-XPS N 1s spectra for thin-film SPAN. This species is absent in electrodes with carbon additives. Moreover, the C 1s spectra for thin-film SPAN (Figure S9b) feature a lower amount of sp^2 C═C species (<284 eV). A plausible explanation is that some of the sp^2 C═C carbon in thin-film SPAN are converted to sp^3 carbon in C−Li after the 1st discharge.

Figure 3e summarizes the mechanism for the formation of N−Li and C−Li intermediates and the role of conductive carbon in eliminating them. It is noticeable that extra electrons participate in the conversion reaction from intermediates to the discharge products. As a result, the presence of conductive carbon is essential for realizing the full capacity of SPAN.

2.4. Structure of SPAN after the 1st Cycle. We then examine the change in electronic/molecular structure during the 1st cycle. The loss/conversion of nonaromatic sulfur/nitrogen is associated with an increase in the degree of conjugation. In principle, this should lead to an increase in electrical conductivity. This is indeed confirmed by the measurement of the pristine and the 1st charged SPAN thin films (Figure 4a,b). After the 1st charge, the SPAN

https://doi.org/10.1021/jacs.3c00628
J. Am. Chem. Soc. XXXX, XXX, XXX−XXX

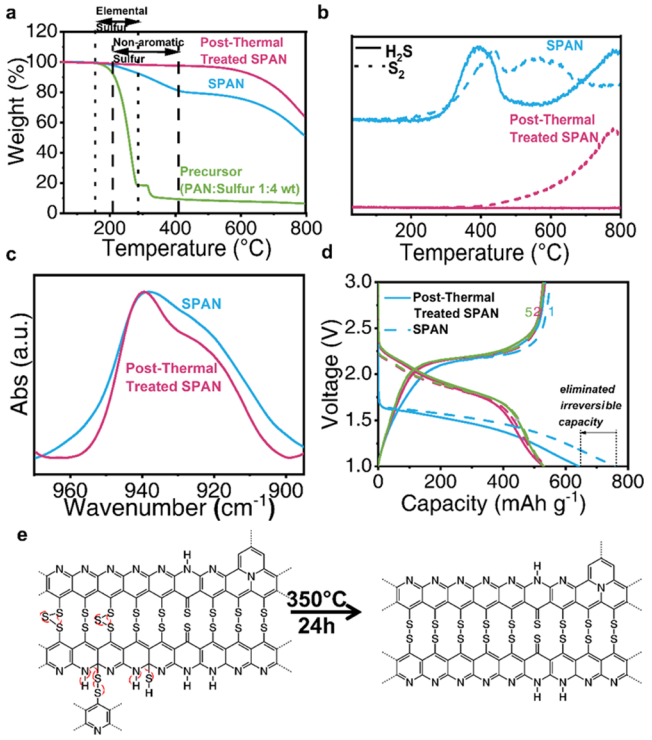

Figure 6. Reducing the 1st discharge irreversible capacity loss in the SPAN battery by a post-thermal treatment method. (a) Thermal gravimetric analysis (TGA); (b) TGA–mass spectrometry (TGA–MS) results for mass traces at m/z = 34 (H_2S) and 64 (S_2); (c) C–S bond FTIR for the SPAN before and after post-thermal treatment; (d) discharge/charge profiles for SPAN before and after post-thermal treatment at 0.2C (1C = 600 mAh g_{SPAN}^{-1}); and (e) proposed structural change for SPAN before and after post-thermal treatment.

conductivity increases by 2 orders of magnitude (from 1.21 × 10^{-7} to 4.43 × 10^{-5} S cm^{-1}). The ultraviolet photoelectron spectroscopy (UPS) results, as shown in Figure S10, indicate that there is an over 4 eV valence band maximum (VBM) shift between the pristine and charged SPAN. The enhanced electrical conductivity and shifted VBM are indicative of the extension of the SPAN conjugation structure.

We next consider the redox reaction for the reversible capacity, mainly concerning whether Li_2S is a major discharge product (Figure S11).[11] The Raman spectra (Figure 4c) show no sign of Li_2S, confirming that it is at most a byproduct from nonaromatic sulfur components. Instead, a lithiated fused (thio)-pyridine chain is the main product after discharge (Figure 4d). This result agrees with Ming et al.[27] A more detailed discussion regarding the Raman spectra is included in the Supporting Information, "SPAN Raman Spectra Analysis" section.

The proposed structure for the main charged product is shown in Figure 4d. The C–S and S–S peaks reappear after charge but with reduced relative intensity. This observation is consistent with the earlier discussion regarding the irreversible loss of sulfur (as H_2S). Though SPAN after the 1st charge has more aromatic components compared to the pristine material, the steric effects between the fused pyridine chains and S–S chains prevent the formation of a planar structure, hence a stronger D band than the G band.

2.5. Proposed Reaction Mechanism for SPAN. Based on the above discussion, we propose a working mechanism for the 1st and subsequent cycling of SPAN (Figure 5). The role of each functional group is summarized in Figure 5a. During the 1st discharge (Figure 5b), the aromatic functional groups contribute to the reversible capacity, while the irreversible capacity loss is due to the transformation of the nonaromatic functional groups. After the 1st discharge, they will either form H_2S that results in a capacity loss or dissociate from the polymer chain (Li_2S) that results in a capacity partial loss, or convert into the aromatic functional group that results in capacity retention. Furthermore, the conductive carbon is crucial for completing the irreversible transformation. Otherwise, the intermediates (N–Li and C–Li components) will remain in SPAN. The formation of a more aromatic conjugated structure leads to an increased electrical conductivity and subsequently highly reversible cycling (Figure 5b).

2.6. Reducing the 1st Cycle Irreversible Capacity Loss. The understanding of the 1st cycle irreversible capacity loss prompts the question that whether the SPAN synthesis can be modified to reduce irreversibility. Our hypothesis is that post-thermal annealing could be effective. SPAN has residual hydrogen and polysulfide chains. An intrapolymer elimination of H_2S is certainly possible.

Thermal gravimetric analysis (TGA) is applied to determine the proper temperature for SPAN post-thermal treatment (Figure 6a). For the SPAN precursor, the mixture loses 80% weight between 155 and 280 °C, which is consistent with sulfur vaporization. In contrast, SPAN loses 20% of its weight between 210 and 410 °C. We thus select 350 °C as the temperature to eliminate the less stable sulfur component while preventing further SPAN decomposition. TGA for the treated SPAN shows no weight loss before 410 °C. In Figure 6b, TGA–mass spectrometry (TGA–MS) results show that the pristine SPAN starts to release H_2S gas from 250 °C, which is not experienced by the post-treated SPAN. This result agrees with our hypothesis that an intrapolymer elimination of H_2S takes place during the post-thermal treatment process. There is also some sulfur loss in the pristine SPAN at above 210 °C, which could be attributed to the loss of long-chain sulfur. The elemental analysis results listed in Table S1 show that the H/N ratio decreases from 0.49 to 0.27 upon post-treatment, while the S/N ratio decreases from 1.21 to 1.06. The remaining hydrogen in the post-treated SPAN is either from the N–H group or at the end group for each polymer chain. FTIR (Figure 6c) indicates that the nonaromatic C–S component has decreased as compared to the pristine SPAN. The decreased full width at half-maximum (FWHM) also indicates the reduced sulfur components.

SPAN with or without post-treatment was then tested electrochemically (Figure 6d). Both samples show a nearly identical reversible capacity of over 520 mAh g_{SPAN}^{-1}. However, in the 1st cycle, there is only a ~100 mAh g^{-1} irreversible capacity loss for the post-treated SPAN. In comparison, this value is 225 mAh g^{-1} for the reference SPAN. Post-thermal treatment thus eliminates over 50% of irreversible capacity loss. Based on these results, a mechanism for the SPAN intrapolymer elimination of H_2S and sulfur through post-thermal treatment is proposed in Figure 6e. Additional optimization through molecular modification is expected to reduce the irreversibility even further.

3. CONCLUSIONS

We have analyzed the 1st cycle reaction mechanism of SPAN using an array of tools. These analyses are performed on both

https://doi.org/10.1021/jacs.3c00628
J. Am. Chem. Soc. XXXX, XXX, XXX–XXX

common powder electrodes as well as a thin-film electrode that is free of binder and additives, which enables analysis of the spatial distribution of the reaction products. The SPAN functional groups and their roles during the 1st cycle and subsequent cycles are identified. The loss or conversion of the nonaromatic functional groups such as C−S (H_2S formation), C═S (convert to aromatic C−S), and N−H (convert to pyridine-*N*) is responsible for the irreversible capacity loss or structural change during the 1st cycle. Conductive carbon is found to actively participate in the conversion of SPAN intermediates to the discharge products. Based on this understanding, post-thermal treatment is found to reduce the amount of nonaromatic functional groups and over 50% of irreversible capacity loss. During the subsequent cycles, Li^+ is hosted by the electrons near S or N atoms. Due to the high aromaticity of SPAN after 1st cycle, the conjugated structure enables a highly reversible electrochemical process. This study demonstrates the necessity for minimizing the nonaromatic functional groups in SPAN during synthesis. Future directions for eliminating the irreversible capacity include the use of low-hydrogen precursors or more aggressive dehydrogenation agents. Raising the reversible capacity of SPAN based on the proposed structure is challenging since most of the active sites have been utilized during lithiation. However, the introduction of more sulfur through molecular modification (e.g., slightly extending the length of S−S bonds) is possible to enhance the reversible capacity while preserving the cycling stability of SPAN. We believe that the principles presented in this work are applicable to other related sulfurized polymers as well.

■ ASSOCIATED CONTENT

Supporting Information

The Supporting Information is available free of charge at https://pubs.acs.org/doi/10.1021/jacs.3c00628.

Experimental section; characterizations; detailed discussion for SPAN structure reconstruction; thin-film SPAN synthesis and characterizations; and SPAN Raman spectra analysis (PDF)

■ AUTHOR INFORMATION

Corresponding Authors

Ying Shirley Meng − *Department of Nanoengineering, University of California, San Diego, La Jolla, California 92093, United States; Materials Science and Engineering Program, University of California, San Diego, La Jolla, California 92093, United States; Pritzker School of Molecular Engineering, University of Chicago, Chicago, Illinois 60637, United States;* orcid.org/0000-0001-8936-8845; Email: shirleymeng@uchicago.edu

Ping Liu − *Department of Nanoengineering, University of California, San Diego, La Jolla, California 92093, United States; Materials Science and Engineering Program, University of California, San Diego, La Jolla, California 92093, United States;* orcid.org/0000-0002-1488-1668; Email: piliu@ucsd.edu

Authors

Shen Wang − *Department of Nanoengineering, University of California, San Diego, La Jolla, California 92093, United States;* orcid.org/0000-0003-3826-4397

Bingyu Lu − *Department of Nanoengineering, University of California, San Diego, La Jolla, California 92093, United States*

Diyi Cheng − *Department of Nanoengineering, University of California, San Diego, La Jolla, California 92093, United States;* orcid.org/0000-0003-1616-9209

Zhaohui Wu − *Department of Nanoengineering, University of California, San Diego, La Jolla, California 92093, United States*

Shijie Feng − *Materials Science and Engineering Program, University of California, San Diego, La Jolla, California 92093, United States*

Minghao Zhang − *Department of Nanoengineering, University of California, San Diego, La Jolla, California 92093, United States*

Weikang Li − *Department of Nanoengineering, University of California, San Diego, La Jolla, California 92093, United States*

Qiushi Miao − *Materials Science and Engineering Program, University of California, San Diego, La Jolla, California 92093, United States*

Maansi Patel − *Department of Nanoengineering, University of California, San Diego, La Jolla, California 92093, United States*

Jiaqi Feng − *Department of Nanoengineering, University of California, San Diego, La Jolla, California 92093, United States*

Emma Hopkins − *Department of Nanoengineering, University of California, San Diego, La Jolla, California 92093, United States*

Jianbin Zhou − *Department of Nanoengineering, University of California, San Diego, La Jolla, California 92093, United States*

Saurabh Parab − *Materials Science and Engineering Program, University of California, San Diego, La Jolla, California 92093, United States*

Bhargav Bhamwala − *Department of Nanoengineering, University of California, San Diego, La Jolla, California 92093, United States*

Boryann Liaw − *Energy and Environmental Science and Technology Directorate, Idaho National Laboratory, Idaho Falls, Idaho 83415, United States;* orcid.org/0000-0001-7431-1977

Complete contact information is available at: https://pubs.acs.org/10.1021/jacs.3c00628

Author Contributions

⊥S.W. and B.L. contributed equally to this paper.

Notes

The authors declare no competing financial interest.

■ ACKNOWLEDGMENTS

This work was supported by the Office of Vehicle Technologies of the U.S. Department of Energy through the Advanced Battery Materials Research (BMR) Program (Battery500 Consortium) under Contract DE-EE0007764 and PNNL-595241. Part of the work used the UCSD-MTI Battery Fabrication Facility and the UCSD-Arbin Battery Testing Facility. FIB and TEM characterizations were performed at the San Diego Nanotechnology Infrastructure (SDNI) of UCSD, a member of the National Nanotechnology Coordinated Infrastructure, which is supported by the National

Science Foundation (Grant ECCS1542148). The use of FTIR and Raman facilities was supported by NSF through the UC San Diego Materials Research Science and Engineering Center (UCSD MRSEC), grant #DMR-201192. The authors acknowledge the use of facilities and instrumentation at the UC Irvine Materials Research Institute (IMRI), which is supported in part by the National Science Foundation through the UC Irvine Materials Research Science and Engineering Center (DMR-2011967). XPS and UPS experiments were performed using instrumentation funded in part by the National Science Foundation Major Research Instrumentation Program under grant no. CHE-1338173.

REFERENCES

(1) Zhang, X.; Chen, K.; Sun, Z.; Hu, G.; Xiao, R.; Cheng, H.-M.; Li, F. Structure-Related Electrochemical Performance of Organosulfur Compounds for Lithium−Sulfur Batteries. *Energy Environ. Sci.* **2020**, *13*, 1076−1095.

(2) Pang, Q.; Liang, X.; Kwok, C. Y.; Nazar, L. F. Advances in Lithium−Sulfur Batteries Based on Multifunctional Cathodes and Electrolytes. *Nat. Energy* **2016**, *1*, No. 16132.

(3) Shim, J.; Striebel, K. A.; Cairns, E. J. The Lithium/Sulfur Rechargeable Cell. *J. Electrochem. Soc.* **2002**, *149*, No. A1321.

(4) Yin, Y.-X.; Xin, S.; Guo, Y.-G.; Wan, L.-J. Lithium-Sulfur Batteries: Electrochemistry, Materials, and Prospects. *Angew. Chem., Int. Ed.* **2013**, *52*, 13186−13200.

(5) Zhao, M.; Li, B.; Peng, H.; Yuan, H.; Wei, J.; Huang, J. Lithium−Sulfur Batteries under Lean Electrolyte Conditions: Challenges and Opportunities. *Angew. Chem., Int. Ed.* **2020**, *59*, 12636−12652.

(6) Tang, C.; Zhang, Q.; Zhao, M.-Q.; Huang, J.-Q.; Cheng, X.-B.; Tian, G.-L.; Peng, H.-J.; Wei, F. Nitrogen-Doped Aligned Carbon Nanotube/Graphene Sandwiches: Facile Catalytic Growth on Bifunctional Natural Catalysts and Their Applications as Scaffolds for High-Rate Lithium-Sulfur Batteries. *Adv. Mater.* **2014**, *26*, 6100−6105.

(7) Song, J.; Gordin, M. L.; Xu, T.; Chen, S.; Yu, Z.; Sohn, H.; Lu, J.; Ren, Y.; Duan, Y.; Wang, D. Strong Lithium Polysulfide Chemisorption on Electroactive Sites of Nitrogen-Doped Carbon Composites For High-Performance Lithium-Sulfur Battery Cathodes. *Angew. Chem.* **2015**, *127*, 4399−4403.

(8) Xiao, L.; Cao, Y.; Xiao, J.; Schwenzer, B.; Engelhard, M. H.; Saraf, L. V.; Nie, Z.; Exarhos, G. J.; Liu, J. A Soft Approach to Encapsulate Sulfur: Polyaniline Nanotubes for Lithium-Sulfur Batteries with Long Cycle Life. *Adv. Mater.* **2012**, *24*, 1176−1181.

(9) Fu, Y.; Manthiram, A. Core-Shell Structured Sulfur-Polypyrrole Composite Cathodes for Lithium-Sulfur Batteries. *RSC Adv.* **2012**, *2*, 5927−5929.

(10) Wang, X.; Yang, Y.; Lai, C.; Li, R.; Xu, H.; Tan, D. H. S.; Zhang, K.; Yu, W.; Fjeldberg, O.; Lin, M.; Tang, W.; Meng, Y. S.; Loh, K. P. Dense-Stacking Porous Conjugated Polymer as Reactive-Type Host for High-Performance Lithium Sulfur Batteries. *Angew. Chem., Int. Ed.* **2021**, *60*, 11359−11369.

(11) Wang, J.; Yang, J.; Wan, C.; Du, K.; Xie, J.; Xu, N. Sulfur Composite Cathode Materials for Rechargeable Lithium Batteries. *Adv. Funct. Mater.* **2003**, *13*, 487−492.

(12) Wei, S.; Ma, L.; Hendrickson, K. E.; Tu, Z.; Archer, L. A. Metal-Sulfur Battery Cathodes Based on PAN-Sulfur Composites. *J. Am. Chem. Soc.* **2015**, *137*, 12143−12152.

(13) Liu, H.; Holoubek, J.; Zhou, H.; Chen, A.; Chang, N.; Wu, Z.; Yu, S.; Yan, Q.; Xing, X.; Li, Y.; Pascal, T. A.; Liu, P. Ultrahigh Coulombic Efficiency Electrolyte Enables Li||SPAN Batteries with Superior Cycling Performance. *Mater. Today* **2021**, *42*, 17−28.

(14) Ma, S.; Zuo, P.; Zhang, H.; Yu, Z.; Cui, C.; He, M.; Yin, G. Iodine-Doped Sulfurized Polyacrylonitrile with Enhanced Electrochemical Performance for Room-Temperature Sodium/Potassium Sulfur Batteries. *Chem. Commun.* **2019**, *55*, 5267−5270.

(15) Lei, J.; Chen, J.; Naveed, A.; Zhang, H.; Yang, J.; Nuli, Y.; Wang, J. Sulfurized Polyacrylonitrile Cathode Derived from Intermolecular Cross-Linked Polyacrylonitrile for a Rechargeable Lithium Battery. *ACS Appl. Energy Mater.* **2021**, *4*, 5706−5712.

(16) Wu, Z.; Bak, S. M.; Shadike, Z.; Yu, S.; Hu, E.; Xing, X.; Du, Y.; Yang, X. Q.; Liu, H.; Liu, P. Understanding the Roles of the Electrode/Electrolyte Interface for Enabling Stable Li||Sulfurized Polyacrylonitrile Batteries. *ACS Appl. Mater. Interfaces* **2021**, *13*, 31733−31740.

(17) Chen, X.; Peng, L.; Wang, L.; Yang, J.; Hao, Z.; Xiang, J.; Yuan, K.; Huang, Y.; Shan, B.; Yuan, L.; Xie, J. Ether-Compatible Sulfurized Polyacrylonitrile Cathode with Excellent Performance Enabled by Fast Kinetics via Selenium Doping. *Nat. Commun.* **2019**, *10*, No. 1021.

(18) Trevey, J. E.; Gilsdorf, J. R.; Stoldt, C. R.; Lee, S.-H.; Liu, P. Electrochemical Investigation of All-Solid-State Lithium Batteries with a High Capacity Sulfur-Based Electrode. *J. Electrochem. Soc.* **2012**, *159*, A1019−A1022.

(19) Wang, J.; Yang, J.; Xie, J.; Xu, N. A Novel Conductive Polymer-Sulfur Composite Cathode Material for Rechargeable Lithium Batteries. *Adv. Mater.* **2002**, *14*, 963−965.

(20) Chang, Z.; Dou, H.; Ding, B.; Wang, J.; Wang, Y.; Xu, G.; Li, C. Interconnected Core-Shell Pyrolyzed Polyacrylonitrile@sulfur/Carbon Nanocomposites for Rechargeable Lithium-Sulfur Batteries. *New J. Chem.* **2016**, *40*, 7680−7686.

(21) Doan, T. N. L.; Ghaznavi, M.; Konarov, A.; Zhang, Y.; Chen, P. Cyclability of Sulfur/Dehydrogenated Polyacrylonitrile Composite Cathode in Lithium-Sulfur Batteries. *J. Solid State Electrochem.* **2014**, *18*, 69−76.

(22) Yu, X. G.; Xie, J. Y.; Yang, J.; Huang, H. J.; Wang, K.; Wen, Z. S. Lithium Storage in Conductive Sulfur-Containing Polymers. *J. Electroanal. Chem.* **2004**, *573*, 121−128.

(23) Fanous, J.; Wegner, M.; Grimminger, J.; Andresen, Ä.; Buchmeiser, M. R. Structure-Related Electrochemistry of Sulfur-Poly(Acrylonitrile) Composite Cathode Materials for Rechargeable Lithium Batteries. *Chem. Mater.* **2011**, *23*, 5024−5028.

(24) Huang, C. J.; Cheng, J. H.; Su, W. N.; Partovi-Azar, P.; Kuo, L. Y.; Tsai, M. C.; Lin, M. H.; Panahian Jand, S.; Chan, T. S.; Wu, N. L.; Kaghazchi, P.; Dai, H.; Bieker, P. M.; Hwang, B. J. Origin of Shuttle-Free Sulfurized Polyacrylonitrile in Lithium-Sulfur Batteries. *J. Power Sources* **2021**, *492*, No. 229508.

(25) Weret, M. A.; Jeffrey Kuo, C. F.; Zeleke, T. S.; Beyene, T. T.; Tsai, M. C.; Huang, C. J.; Berhe, G. B.; Su, W. N.; Hwang, B. J. Mechanistic Understanding of the Sulfurized-Poly(Acrylonitrile) Cathode for Lithium-Sulfur Batteries. *Energy Storage Mater.* **2020**, *26*, 483−493.

(26) Huang, C. J.; Lin, K. Y.; Hsieh, Y. C.; Su, W. N.; Wang, C. H.; Brunklaus, G.; Winter, M.; Jiang, J. C.; Hwang, B. J. New Insights into the N-S Bond Formation of a Sulfurized-Polyacrylonitrile Cathode Material for Lithium-Sulfur Batteries. *ACS Appl. Mater. Interfaces* **2021**, *13*, 14230−14238.

(27) Wang, W.; Cao, Z.; Elia, G. A.; Wu, Y.; Wahyudi, W.; Abou-Hamad, E.; Emwas, A. H.; Cavallo, L.; Li, L. J.; Ming, J. Recognizing the Mechanism of Sulfurized Polyacrylonitrile Cathode Materials for Li-S Batteries and beyond in Al-S Batteries. *ACS Energy Lett.* **2018**, *3*, 2899−2907.

(28) Perez Beltran, S.; Balbuena, P. B. Sulfurized Polyacrylonitrile (SPAN): Changes in Mechanical Properties during Electrochemical Lithiation. *J. Phys. Chem. C* **2021**, *125*, 13185−13194.

(29) Wang, X.; Qian, Y.; Wang, L.; Yang, H.; Li, H.; Zhao, Y.; Liu, T. Sulfurized Polyacrylonitrile Cathodes with High Compatibility in Both Ether and Carbonate Electrolytes for Ultrastable Lithium−Sulfur Batteries. *Adv. Funct. Mater.* **2019**, *29*, No. 1902929.

(30) Jin, Z.-Q.; Liu, Y.-G.; Wang, W.-K.; Wang, A.-B.; Hu, B.-W.; Shen, M.; Gao, T.; Zhao, P.-C.; Yang, Y.-S. A New Insight into the Lithium Storage Mechanism of Sulfurized Polyacrylonitrile with No Soluble Intermediates. *Energy Storage Mater.* **2018**, *14*, 272−278.

(31) Shen, Y.; Zhang, J.; Pu, Y.; Wang, H.; Wang, B.; Qian, J.; Cao, Y.; Zhong, F.; Ai, X.; Yang, H. Effective Chemical Prelithiation Strategy for Building a Silicon/Sulfur Li-Ion Battery. *ACS Energy Lett.* **2019**, *4*, 1717−1724.

https://doi.org/10.1021/jacs.3c00628
J. Am. Chem. Soc. XXXX, XXX, XXX−XXX

(32) Wang, S.; Cabreros, A.; Yang, Y.; Hall, A. S.; Valenzuela, S.; Luo, Y.; Correa-Baena, J.-P.; Kim, M.; Fjeldberg, Ø.; Fenning, D. P.; Meng, Y. S. Impacts of the Hole Transport Layer Deposition Process on Buried Interfaces in Perovskite Solar Cells. *Cell Rep. Phys. Sci.* **2020**, *1*, No. 100103.

https://doi.org/10.1021/jacs.3c00628
J. Am. Chem. Soc. XXXX, XXX, XXX−XXX